

Scenarios for protein aggregation: Molecular Dynamics simulations and Bioinformatic Analysis

Ruxandra I. Dima¹, Bogdan Tarus², John E. Straub² and D. Thirumalai^{3,4}

¹ Department of Chemistry, University of Cincinnati, Cincinnati, OH 45221

² Department of Chemistry, Boston University, Boston, MA 02215,

³Biophysics Program, Institute for Physical Science and Technology

⁴Department of Chemistry and Biochemistry

University of Maryland, College Park, MD 20742

(Dated: November 12, 2018)

Abstract

Introduction:

Increasing number of diseases including Alzheimer's disease [1], transmissible prion disorders [2], type II diabetes are linked to amyloid fibrils [3]. The mechanism of amyloid fibril formation starting from the monomer is still poorly understood. During the cascade of events in the transition from monomers to mature fibrils a number of key intermediates, namely, soluble oligomers and protofilaments are populated. It is suspected that the conformations of the peptides in these aggregated state differ substantially from the isolated monomer which implies that the monomer undergoes substantial inter-peptide interaction-driven structural transformations [4]. The need to understand the assembly kinetics of fibril formation has become urgent because of the realization that soluble oligomers of amyloidogenic peptides may be even more neurotoxic than the end product, namely, the amyloid fibrils [5]. In order to fully understand the routes to fibril formation one has to characterize the major species in the assembly pathways. The characterization of the energetics and dynamics of oligomers (dimers, trimers etc) is difficult using experiments alone because they undergo large conformational fluctuations. In this context, carefully planned molecular dynamics simulation studies [6, 7, 8, 9], computations using coarse-grained models [10], and bioinformatic analysis [11, 12] have given considerable insights into the early events in the route to fibril formation. Here, we describe progress along this direction using examples taken largely from our own work.

In this chapter, we focus on the following aspects of protein aggregation using $A\beta$ -peptides and prion proteins as examples.

- What are the plausible scenarios in the transition from monomers to amyloid fibril formation?
- What features of the amyloidogenic peptides control the growth kinetics of fibrils? Although the assembly mechanism is complex the overall growth kinetics is determined largely by the charge states and hydrophobicity of the monomers.
- Can sequence and structural analysis be used to predict specific patterns that are likely to be susceptible to aggregation? By exploiting the sequence profiles and structures of the cellular form of prions, PrP^C , we uncover the regions that are likely to trigger the large conformational changes in the transition from PrP^C to the scrapie form, PrP^{Sc} .
- Is there an organizational principle in oligomer and fibril formation? The formation of

morphologically similar aggregates by a variety of proteins that are unrelated in sequence or structure suggests that certain general principles may govern fibrillization. However, the vastness of sequence space and the heterogeneity of environmentally-dependent interactions make deciphering the principles of aggregation difficult. Nevertheless, we will argue that oligomers and higher order structures form in such a way that the number of intra- and inter-molecular hydrophobic interactions are maximized and electrostatic repulsions are minimized. The latter implies that the motifs that minimize the number of salt bridges are preferred.

For the issues raised above we formulate tentative ideas using phenomenological arguments and atom molecular dynamics (MD) simulations. Using a number of experimental observations and results from computer simulations certain general principles of amyloid formation seem to be emerging. There are a number of unresolved issues that remain despite significant progress. A few of these are outlined at the end of the paper.

Scenarios for peptide-association:

The molecular details of the cascade of events that lead to the formation of amyloid fibrils remain unknown because the species along the aggregation pathways are highly dynamic and metastable. Indeed, AFM images of protofibrils show that they undergo shape fluctuations which implies a heterogeneous population of species. A number of experimental studies suggest that fibril formation exhibits all the characteristics of a nucleation growth process. It is suspected that the formation of a critical nucleus is the rate determining step in the fibril formation [13]. Once the critical nucleus, whose very nature might be both depend on sequence as well as external conditions, forms the fibril formation process is essentially downhill in free energy. The nucleation characteristics manifests themselves in the appearance of a lag phase in the fibril formation. The lag phase disappears if a seed or a preformed nucleus is present in the saturated peptide solution. The seeded growth of fibrils has also been observed in simple lattice and off-lattice models of protofibril formation. From this perspective the general scenario for explaining aggregation kinetics is in place. However, the details of the process including the dependence of the growth kinetics on the specifics of the sequence are not fully understood.

Here we present two extreme scenarios [14] that describe the needed conformational changes in monomers that lead to a population of species that can nucleate and grow. The two potential

scenarios, which follow from the energy landscape perspective of aggregation, differ greatly in the description of the dynamics of the monomers. It was advocated early on that fibrillization requires partial unfolding of the native state [15] or partial folding of the unfolded state (see Scenario I in Fig. (1)). Both events, which are likely to involve crossing free energy barriers lead to the transient population of the assembly-competent structures \mathbf{N}^* . The better appreciated possibility is Scenario I in which environmental fluctuations (pH shifts for example) produces spontaneously the \mathbf{N}^* conformation. For example, extensive experiments [16] have shown that the \mathbf{N}^* state in transthyretin (TTR), which has a higher free energy than the native state \mathbf{N} , formed upon unraveling of the strands C and D at the edge of the structure. This process exposes an aggregation-prone strand B. One can also envision a scenario in which \mathbf{N}^* has a lower free energy than \mathbf{N} thus making the folded (functional state) state metastable. It is likely that amyloidogenic proteins, in which nearly complete transformation the structure takes place upon fibrillization, may follow the second scenario. In both cases fibrillization kinetics results from the ability to populate the \mathbf{N}^* species. In either scenarios (TTR aggregation that follows Scenario I or PrP^{Sc} formation that follows scenario II) growth kinetics is initially determined by the 'unfolding' barriers separating \mathbf{N}^* from either \mathbf{N} or \mathbf{U} . The energy-landscape perspective for aggregation (Fig. (1)) suggests that the free energy of stability may not be a good indicator of fibril growth kinetics. Rather, growth kinetics should correlate with unfolding barriers.

In scenario I, the amyloidogenic state \mathbf{N}^* is formed by denaturation stress or other environmental fluctuations. The production of \mathbf{N}^* in scenario II can occur by two distinct routes. If \mathbf{N} is metastable, as is apparently the case for PrP^c [17], then conformational fluctuations can lead to \mathbf{N}^* . Alternatively, formation of \mathbf{N}^* can also be triggered by intermolecular interactions. In the latter case \mathbf{N}^* can only form when the protein concentration exceeds a threshold value. As noted below there is evidence for both scenarios in the routes to fibril states.

In order to understand the kinetics of fibrillization it is necessary to characterize the early events and pathways that lead to the formation of the critical nucleus. In terms of the energy landscape, the structures of \mathbf{N}^* , the ensemble of transition state structures, and the conformations of the critical nuclei must be known to fully describe the assembly kinetics. Teplow and coworkers, who have followed the growth of fibrils for eighteen peptides, including $A\beta_{1-40}$ and $A\beta_{1-42}$ [18] showed that the formation of amyloids is preceded by the transient population of the

intermediate oligomeric state with high α -helical content. This is remarkable given that both the monomers and fibrils have little or no α -helical content. Therefore, the transient formation of α -helical structure represent an on-pathway intermediate state.

Somewhat surprisingly, we found using multiple long MD simulations that in the oligomerization of $A\beta_{16-22}$ peptides [6] the oligomer assembles into antiparallel β -structure upon inter-peptide interactions. Even in the oligomerization of these small peptides from the $A\beta$ family the assembly was preceded by the formation of an on-pathway α -helical intermediate. Based on our findings and the work by Teplow and coworkers we postulated that the formation of oligomers rich in α -helical structure may be a universal mechanism for $A\beta$ peptides.

Formation of the on-pathway α -helical intermediate may be rationalized using the following arguments. The initial events involve the formation of "non-specific" oligomers driven by hydrophobic interactions that reduces the effective available volume to each $A\beta$ peptide. In the confined space peptides adopt α -helical structure. Further structural changes are determined by the requirement of maximizing the number of favorable hydrophobic and electrostatic interactions. Provided that $A\beta$ oligomers contains large number of peptides, this can be achieved if $A\beta$ peptides adopt extended β -like conformations.

There is some similarity between the aggregation mechanism postulated for $A\beta$ peptides and the nucleated conformational conversion (NCC) model envisioned for the conversion of Sup35 to $[PSI^+]$ in *Saccharomyces Cerevisiae* [19]. By studying the assembly kinetics of Sup35, Serio *et al.* [20] proposed the NCC model, which combines parts of the templated assembly and nucleation-growth mechanisms. The hallmark of the NCC model [20] is the formation of a critical sized mobile oligomer, in which Sup35 adopts a conformation that may be distinct from its monomeric random coil or the one it adopts in the aggregated state. The formation of a critical nucleus to which other Sup35 can assemble involves a conformational change to states that it adopts in the self-propagating $[PSI^+]$. The α helical intermediate seen in $A\beta$ peptides may well correspond to the mobile oligomer that has the "wrong" conformation to induce further assembly.

Assembly of $A\beta_{16-22}$ oligomers:

The $A\beta_{16-22}$ monomer is a random coil: The small size of $A\beta_{16-22}$ peptides, which adopt an

antiparallel β -sheet structure in the fibril state, is an ideal system for exploring in detail the mechanism of oligomer formation. Using fairly long and multiple trajectories [6], the assembly pathways for $3 A\beta_{16-22} \rightarrow (A\beta_{16-22})_3$ were probed using all atom simulations in explicit water. The simulations of $A\beta_{16-22}$ and the corresponding mutants allowed us to draw a number of conclusions that may be of general validity.

The simulations of the $A\beta_{16-22}$ monomer at room temperature and at neutral pH showed that it is predominantly a random coil. The finite size of the system gives rise to large conformational fluctuations that lead to the population of strand-like structures. There is a very low ($\sim 3\%$) probability of α -helical conformations. The study of this simple system shows that the β -sheet conformation adopted by the monomer must be due to interactions with other peptides.

Oligomerization of three $A\beta_{16-22}$ peptides requires a transient monomeric α -helical intermediate: Upon interaction with other peptides substantial changes in the conformations of the individual monomers occur. The size of the monomer increases by about 50%. More surprisingly, we found that as interpeptide interaction increases there is a dramatic increase in the percentage of α -helical content during intermediate times. At longer times the monomer undergoes a $\alpha \rightarrow \beta$ transition. Due to the small size of the oligomer ($n = 3$) there are substantial conformational fluctuations even after the three strands are roughly in antiparallel registry. Nevertheless, the simulations showed that the size of the nucleus for $A\beta_{16-22}$ cannot be large because even with $n = 3$ there are signatures of stable oligomers. Indeed, explicit simulations for $t > 300$ ns show that one can obtain nearly perfectly aligned $A\beta_{16-22}$ trimers in which the strands are in antiparallel registry (Li, private communication). In these simulations $\langle \hat{u}_i(t)\hat{u}_j(t) \rangle$ where $\hat{u}_i(t)$ is the unit vector connecting the N and C termini of peptide i fluctuates around values close to -1.

The dominant pathway for $3 A\beta_{16-22} \rightarrow (A\beta_{16-22})_3$ from the simulations showed that in the intermediate stages the monomer transiently populates an α -helix (see Fig.(8) from [6]). It should be emphasized that in the assembly process (especially in the early stages in the oligomerization) there are multiple routes. As a result, kinetic trapping can result in structures that are not conducive to forming the most stable antiparallel structures. Such kinetically controlled structures have been explicitly probed in dimer formation of small fragments of $A\beta$ peptides.

These studies and other simulations illustrate the complexity in dissecting the assembly of even small amyloidogenic peptides into ordered structures.

The gross features of the fibril structures of a number of proteins and peptides whose monomer sequences and structures are unrelated are similar. This observation might suggest that the interactions that stabilize the oligomers and fibrils must be “universal” involving perhaps only backbone hydrogen bonds. It might appear that side chains, and hence sequence differences, might play a secondary role. Such a conclusion is further supported by repeated observations [21] that any protein or peptide can be made to form cross- β structures under appropriate conditions. However, experiments [22] and simulations [7, 23] show that side chain interactions are crucial in directing oligomer formation. Trimers of $A\beta_{16-22}$ are stabilized primarily by favorable inter-peptide hydrophobic interactions between residues in the central hydrophobic cluster (LVFFA) and secondary by inter-peptide salt bridge formation between K and E.

The importance of side chains can be demonstrated by examining the effect of mutations on the trimer formation in $A\beta_{16-22}$ peptides. We showed using simulations that the mutant GLVFFAK, which eliminates the formation of intermolecular salt-bridge entirely destabilizes the trimer. Similarly replacement of L, F, F by S, also destabilizes the trimer. These simulations show that the sequence plays a key role in the tendency of peptides to form amyloid fibrils. Although no general role has emerged it seems that sequences with enhanced correlation between charges [12] or preponderance of contiguous (> 3) hydrophobic residues might be amenable to amyloid formation on finite time scales.

Dimerization of $A\beta_{10-35}$ peptides:

Generation of putative dimer structures: In contrast to $A\beta_{16-22}$ fibrils the longer peptide $A\beta_{10-35}$ adopts a parallel β -sheet conformation in the amyloid state. It is now suspected that in the fibril state the monomer is stabilized by an intra-molecular salt bridge between Asp23 and Lys28. In order for this salt bridge to form there has to be a bend in the monomeric structures involving the residues VGSN. The importance of a stable turn, which was experimentally determined in the NMR structures, was emphasized in MD simulations as well.

In a recent study [8], we used a number of computational methods to probe dimer formation. We first generated a putative set of dimer conformations that is based on shape complementarity.

The work on $A\beta_{16-22}$ showed that both inter-peptide hydrophobic interactions and the creation of favorable electrostatic contacts are required to produce marginally stable oligomers. In order to dissect their relative importance we generated two homodimer decoy sets by maximizing the number of contacts between the monomer interfaces. The first 2000 dimer structures of each set were selected by minimizing the interaction energy between the monomers. In order to distinguish between desolvation and electrostatic interactions we used two distinct energy functions. The φ -dimer (Fig. (2(a))) minimizes the desolvation energies of the dimer at the interface whereas the ε -dimer (Fig. (2(b))) corresponds to structures that have the highest inter-peptide electrostatic interactions. The structure of the φ -dimer is dominated by contacts between hydrophobic segments of the monomers. The hydrophobic core, LVFFA(17-21), and the hydrophobic C-terminus of both monomers are buried at the dimer interface. The contacts at the interface of the φ -dimer are conserved over the lowest energy dimer structures. The ε -dimer interface is characterized by electrostatic inter-monomeric interactions, among which the salt bridge Glu11(A)-Lys28(B) has the largest contribution. Contrary to the φ -dimer, the contacts observed at the ε -dimer interface are not conserved across the set of the low energy dimers due to the increased specificity and strength of the electrostatic interaction.

Interior of $A\beta$ oligomers is dry: Insights into the assembly mechanism of the φ -dimer and ε -dimer can be obtained from the Potential of Mean Force (PMF). The PMF for the dimerization process was obtained along the center of mass of the two monomers as the Fig.(3) indicates. For each free energy profile, one can distinguish three distinct intervals. In the outer interval, the PMF value is nearly constant, from 6.5 Å – 7.0 Å to maximum separation, which in our case is 9.0 Å. At a distance of 6.5 Å for the ε -dimer and 7.0 Å for the φ -dimer, the first solvation shells of the monomers come into contact, and for both dimers the energetics of desolvation of the associating monomers is unfavorable. In the second interval for the ε -dimer, the value of the PMF continues to increase up to 1.2 kcal/mol at a 3.0 Å separation; for the φ -dimer, the potential energy reaches a value of 0.8 kcal/mol at 5.5 Å, and after that the desolvation is favorable, ending in an unstable local minimum at 3.0 Å. For the third interval, from 3.0 Å to 0.0 Å, there is only one solvation shell between the monomers. The water molecules are most strongly ordered near the monomers through electrostatic interactions and hydrogen bonds. As

a result, the PMF for the ε -dimer increases sharply between 3.0 Å and 1.3 Å up to 2.4 kcal/mol. At contact, the van der Waals attraction predominates, making the overall dimerization process energetically favorable. For the φ -dimer, the solvation shell between the hydrophobic regions of the monomers is only weakly bound to the solute, and after a small increase in the PMF, corresponding to the van der Waals attraction, the desolvation is entirely favorable.

If the approach along the center of mass of the monomers approximately represents a minimum energy path, then the expulsion of water in the φ -dimer must be an early event in the assembly. Explicit simulations for $A\beta_{16-22}$ oligomers [6] also show that desolvation occurs early. As a result, the interior of $A\beta$ oligomers is dry.

Hydrophobic interactions between monomers are the driving force in the association of $A\beta_{10-35}$ peptides into dimers: Comparing the φ -dimer ε -dimer models for monomer association, we find that the former appears to lead to more energetically favorable dimerization than the latter. It appears to be more efficient to remove the entropically unfavorable structured water between the opposing hydrophobic regions of the two monomers than to stabilize the monomer solely through electrostatic interactions. This is in good agreement with the experimental and MD simulations observation that the mutation E22Q – where a charged glutamic acid residue is replaced by a polar glutamine residue – increases the propensity for amyloid formation [24, 25]. Molecular dynamics simulations of this increased amyloidogenic activity for the E22Q mutant peptide led to the conclusion that the water-peptide interaction is less favorable for the mutant peptide [26]. Following a more detailed analysis of the structure and dynamics of the WT and E22Q $A\beta_{10-35}$, it has suggested that a change in the charge state of the peptide, due to the E22Q mutation, leads to an increase of the hydrophobicity of the peptide that could be responsible for the increased activity [27].

The time evolution of the φ -dimer structure was analyzed and it was observed that the monomers remain in contact during the simulation. It was shown that the hydrophobic interaction between the monomers of the φ -dimer acts as a stabilizing force of the dimer. The “extended core” region 15–30 of both monomers in the φ -dimer makes the principal contribution to the hydrophobic interaction energy. The φ -dimer undergoes internal structural reorganization in the terminal regions of the monomeric peptides. Our simulations indicate that there is substan-

tial reorganization of the peptide monomers in the N- and C-terminus regions, as expected for a dimer weakly and relatively non-specifically stabilized by hydrophobic contacts at the dimer interface. Importantly, the structure of the central hydrophobic cluster LVFFA region assumes a conformation similar to that observed for the monomeric peptide in both experiment[28] and simulation[29]. Our simulations suggest that the preservation of the structure of the LVFFA central hydrophobic cluster plays an important role in the stabilization of the φ -dimer structure.

The finding that the φ -dimer may constitute the ensemble of stable $A\beta_{10-35}$ dimer has important implications for fibril formation. The initial event in the dimerization involves, in all likelihood, contacts between the central hydrophobic clusters. In this process, expulsion of water molecules in the interface might be a key event just as in the oligomerization of $A\beta_{16-22}$ fragments[6]. Since this process involves cooperative rearrangement of ordered water molecules, it is limited by an effective free energy barrier. Based on our results, we conjecture that events prior to the nucleation process themselves might involve crossing free energy barriers which depend on the peptide-peptide and peptide-water interactions (Fig. (1)).

Initial stages in the PrP^C conformational transition:

Prion proteins are extracellular globular proteins which are attached to the plasma membrane by a GPI anchor. They have been linked to various transmissible spongiform encephalopathies (TSEs) including the bovine spongiform encephalopathy, the scrapie disease in sheep, and the Creutzfeldt-Jakob disease in humans. The causative agent in these diseases is believed to be the aggregated form (PrP^{Sc}) of the cellular prion protein (PrP^C) [30]. The transition to the scrapie form involves a large conformational change from the mainly α -helical PrP^C to the PrP^{Sc} state that is rich in β -sheet. According to the “protein-only” hypothesis [2] PrP^{Sc} serves as a template in inducing conformational transitions in PrP^C that can subsequently be added to PrP^{Sc} . The “protein-only” hypothesis implies that the conformational change leading to the PrP^{Sc} formation from the normal cellular form PrP^C may be spontaneous or might involve interactions with unidentified protein X [31]. Prion proteins, encoded by a single gene, consist of about 250 residues of which the first 22 form a signal sequence. This is followed by unstructured, but likely helical, Cu^{2+} binding octarepeats rich in glycine [2]. The NMR [30, 32, 33] and X-ray [34] structure of PrP^C in various species (human, mouse, syrian hamster, bovine, and sheep)

shows that the ordered C-terminal part is composed of a short antiparallel β -sheet that contains 8% of the residues in the (90-231) fragment and three helices representing 48% of the secondary structure (Fig.(4). Fourier transform infrared spectroscopy measurements [35, 36] indicate that PrP^{Sc}(90-231) has 47% β -sheet and 24% α -helical content.

We have suggested using structural, bioinformatic, and molecular dynamics simulations that formation of PrP^{Sc} follows scenario II (see Fig. (1)). This implies that, either spontaneously or in the presence of a seed of PrP^{Sc}, the metastable cellular form, PrP^C, undergoes a transition to the PrP^{C*} state that is capable of further aggregating or adding to an already present PrP^{Sc} particle. Experiments [37] and scenarios of protein aggregation [14] suggest the proposal that the conformational transition involves the formation of PrP^{C*} that is more stable than PrP^C. The transition from the metastable PrP^C \rightarrow PrP^{C*}, which involves crossing a substantial free energy barrier on the order of 20 kcal/mole [17, 38], results in a state that can nucleate and polymerize to the protease resistant form. We also identified the putative regions that are involved in the PrP^C \rightarrow PrP^{C*} transition. Comparison of a number of structural characteristics (such as solvent accessible area, distribution of (Φ, Ψ) angles, mismatches in hydrogen bonds, nature of residues in local and non-local contacts, distribution of regular densities of amino acids, clustering of hydrophobic and hydrophilic residues in helices) between PrP^C structures and a databank of "normal" proteins shows that the most unusual features are found in helix 2 (residues 172-194) followed by helix 1 (residues 144-153) [11]. In particular, the C-terminal residues in H2 are frustrated in their helical state. Application of the recently introduced notion of discordance, namely, incompatibility of the predicted and observed secondary structures, also points to the frustration of H2 not only in the wild type but also in mutants of human PrP^C. This suggests that the instability of PrP^C proteins may play a role in their being susceptible to the profound conformational change.

We showed [11] that, in addition to the previously proposed role for the segment (90-120) and possibly H1, the C-terminus of H2 and possibly N-terminus may play a role in the $\alpha \rightarrow \beta$ transition. Sequence alignments show that helices in avian prion proteins (chicken, duck, crane) are better accommodated in a helical state which might explain the absence of PrP^{Sc} formation over finite time scales in these species. From the analysis it is clear that the conformational fluctuations in the C-terminal end of helix 2 (H2) and in parts of helix 3 (H3) are involved in the

transition to PrP^{C*} . Because the stability of PrP^C arises from the structures in the C-terminal end, the transition to PrP^{C*} requires global unfolding of PrP^C [39] which explains the origin of the high free energy barrier separating PrP^C and PrP^{C*} [11]. NMR experiments [37, 40] showed that conformational fluctuations that originate in the C-terminal part of H2 are essential in the formation of PrP^{C*} . Structural and mutational studies have also shown that the relatively short helix 1 (H1) is stable over a range of pH values and solvent conditions, and hence is unlikely to undergo conformational change in the transition to PrP^{C*} [41, 42, 43].

The required conformational fluctuations in PrP^C needed to populate PrP^{C*} suggest that the earliest event involves extensive unfolding of the monomeric PrP^C . We used results from a database search of sequence patterns in helices of PrP^C and extensive all atom molecular dynamics (MD) simulations of helical fragments from the mouse prion protein (mPrP^C) to shed light on the nature of instabilities that drive the $\text{PrP}^C \rightarrow \text{PrP}^{C*}$ transition [44]. Previously MD simulations have been used to probe other structural aspects of prion proteins including structures of protofibrils [45]. The 10 residue H1, with an unusual sequence pattern (highly charged and presenting the largest percentage of salt bridges in any α -helix in the PDB), remains helical for the duration of the simulation ($\approx 0.09 \mu\text{s}$). The double mutant (D147A,R151A), which eliminates one of the three salt bridges in H1, is less stable than the wild type. Multiple MD trajectories of peptides encompassing H2 and H3 (together with their connecting loop) with intact disulfide bond (Cys179-Cys214) showed that residues in the second half of H2 clustered around positions 187-188 have large conformational flexibility and non-zero preference for β -strand or coil-like structures. Instability in H2 propagates to H3 especially from position 214 onwards. Based on these results, we mapped the plausible structures of the aggregation prone PrP^{C*} . Despite the limitations (short simulation time and the expected variations of results with different force fields) of all atom simulations, different computational approaches yield qualitatively similar results, namely, the initial conformational transition must involve at least partial unfolding of parts of H2 and H3.

Bioinformatic Analysis:

Pattern of charges in H1 is rare: The distribution of $R(+, -)$ for the 2103 helices from the DSMP shows that *no other natural sequence* has as many $(+,-)$ pairs at positions $(i,i+4)$ as H1

from PrP^C. The search of the entire PDBselect database for the H1 charge pattern shows that in only 56 (4.6%) sequences this pattern occurs at least once, with the total number of patterns being 63. If we restrict the search to be the exact pattern of H1, i.e. $i = -$, $i+3 = -$, $i+4 = +$, $i+7 = +$ and $i+8 = -$ the number of sequences is a mere 23 (or 1.9%). Ziegler et al. [43] arrived at a similar conclusion based on a H1 pattern search in PDB. The 23 rare sequence fragments are either α -helical (83%) or in a random coil state (17%). Analysis of the Yeast genome shows that 828 (or 9.2%) of sequences have the general pattern of H1 with only 253 (2.8%) having the exact pattern. In the *E. Coli* genome the numbers are: 158 (3.7%) for the general charge pattern and 51 (1.2%) for the exact match. These results suggest that the sequence of H1 in PrP^C is unusual not only in its high charge content, but also in the *positioning of charges along the sequence*. More importantly, for the 23 proteins with known 3D structures, the exact charge pattern results overwhelmingly in α -helices. Even more interestingly, analysis of the 19 sequences with mostly α -helical structure reveals that the majority (88%) of (+,-) pairs of residues found at positions (i,i+4) form salt bridges. These results indicate that the unusual stability of the short helix H1 is possibly associated with its ability to form the highly stabilizing salt bridges involving (i,i+4) residues.

Pattern of hydrophobicity in H2 is rare: There are very few sequences that share the pattern of hydrophobicity of H2. In PDBAstral40 [46] (proteins in the PDB having at most 40% sequence similarity) there are only 12 (0.2%) such sequences. In the *E Coli* genome the number is 46 (1%), while in the Yeast genome it is 122 (1.4%). Inspection of the structures of the 12 proteins from PDBAstral40, shows that the sequence is never entirely helical! For example, in only 13% of these proteins the last 5 residues are found in a helix. A characteristic pattern seen in H2 from mammalian prion proteins is TTTT (positions 190-193). In the PDBAstral40 this pattern occurs in only 18 proteins, including the prion sequence. In an overwhelming number of these cases (15 of the 18 proteins) the TTTT pattern is found in a strand and/or loop conformation (irrespective of the identity of the flanking amino acids). These results add further support to our proposal [11] that the second half of H2 would be better accommodated in non-helical conformations.

"Frustrated" secondary structural elements may be harbinger of tendency to polymerize The ease of aggregation and the morphology of the aggregates depend not only on the protein concentration, but also on other external conditions such as temperature, pH and salt concentration. Although most proteins can, under suitable conditions, aggregate the observation that several disease causing proteins form amyloid fibrils under physiologically relevant conditions raises the question: Is aggregation or the need to avoid unproductive pathways encoded in the primary sequence itself? It is clear that sequences that contain a patch of hydrophobic residues are prone to form aggregates [47]. However, it is known that contiguous patches (three or more hydrophobic residues) occur with low probability in globular proteins [48]. For example, sequences with five hydrophobic residues (LVFFA in A β peptide) in a row are not well represented. Similarly, it is unusual to find hydrophobic residues concentrated in a specific region of helices such as is found in helix 2 in PrP^C [11].

It is natural to wonder if secondary structure elements bear signatures that could reveal amyloidogenic tendencies. Two studies have proposed that the extent of "frustration" in the secondary structure elements (SSE) may be harbinger of amyloid fibril formation [11, 49]. Because reliable secondary structure prediction requires knowing the context dependent propensities and multiple sequence alignments (such as used in PHD, Profile network from Heidelberg [50]), it is more likely that assessing the extent of frustration in the SSE rather than analysis of sequence patterns is a better predictor of fibril formation. Frustration in SSE is defined as the incompatibility of the predicted (from PHD, for example) secondary structure and the experimentally determined structure [49]. For example, if a secondary structure is predicted to be in a β -strand with high confidence and if that segment is found (by NMR or X-ray crystallography) to be in a helix, then the structure is frustrated (or discordant or mismatched). The α/β discordance, which can be correlated with amyloid formation, can be assessed using the score $S_{\alpha/\beta} = \frac{1}{L} \sum_{i=1}^L (R_i - 5)$, where R_i is the reliability score predicted by PHD at position i of the query sequence, 5 is the mean score, and L is the sequence length. The bounds on $S_{\alpha/\beta}$ are $0 \leq S_{\alpha/\beta} \leq 4$ with maximal frustration corresponding to $S_{\alpha/\beta} = 4$. Similarly, the measure $S_{\beta/\alpha}$ gives the extent of frustration of a stretch that is predicted to be helical and is found experimentally to be a strand. Using $S_{\alpha/\beta}$ and other structural characteristics, one can make predictions of the plausible regions that are most susceptible to

large conformational fluctuations.

PrP^C and *Dpl*: Using the above concept of SSE frustration the 23 residue sequence (QNNFVHD-CVNITIKQHTVTTTTTK) in mouse PrP^C, with a score of 1.83, was assessed to be frustrated or discordant [11]. Other measures of quantifying the structure also showed that the maximal frustration is localized in the second half (C-terminal of H2) [11]. The validity of this prediction finds support in the analysis of mutants of the PRNP gene associated with inherited TSEs (familial CJD, and FFI). According to SWISS-PROT [51] seven disease-causing point mutations (D178N, V180I, T183A, H187R, T188R, T188K, T188A) are localized in H2. We have used the sequence numbering for the mPrP^C. A naive use of propensities to form helices, a la Chou-Fasman [52], would suggest that with the exception of D178N all other point mutations should lead to better helix formation. However, the $S_{\alpha/\beta}$ scores for the mutants are 1.94, 1.80, 1.30, 1.80, 1.54, 1.94, and 1.94 for D178N, V180I, T183A, H187R, T188K, T188R, and T188A respectively. Thus, in all these mutants H2 is frustrated making it susceptible to conformational fluctuations which have to occur prior to fibrillization. The differences in $S_{\alpha/\beta}$, which can be correlated with local stability, suggest that stability alone might not be a good indicator of the kinetics of amyloid formation.

The gene coding for the Doppel protein (Dpl), termed *Prnd* [53], is a paralog of the prion protein gene, *Prnp*, to which it has about 25% identity. Normally, Dpl is not expressed in the central nervous system, but it is up-regulated in mice with knockout *Prnp* gene. In such cases, overexpression of Dpl causes ataxia with Purkinje cell degeneration [53], which in turn can be cured by the introduction of one copy of wild-type PrP mouse gene [54]. NMR studies of the three-dimensional (3D) structure of mouse Dpl [55] showed that it is structurally similar to the structure of PrP^C (Fig. (5)). However, PrP^C and Dpl produce diseases of the central nervous system using very different mechanisms: PrP^C causes disease only after conversion to the PrP^{Sc} form, while simple overexpression of Dpl, with no necessity to form the scrapie form, causes ataxia. The markedly different disease mechanisms of PrP and Dpl would suggest, in light of the findings for PrP^C, that the mouse Dpl (PDB code 1i17) would not be frustrated. Indeed, prediction of secondary structure by PHD [50] on mouse Dpl correlates well with the experimentally derived structure. The only difference between the predicted and the derived

structure in Dpl is found in the first β -strand region which is predicted to be helical by PHD. But the corresponding $S_{\beta/\alpha} = -3.0$ indicating that this α -helix prediction is unreliable as this sequence has low complexity. Also, the analysis of 1i17 with the WHAT CHECK program [56] reveals that, on average, there are only 8 unsatisfied buried hydrogen-bond donors/acceptors representing 7.4% of all residues in mouse Dpl. This is comparable with the average value of 6% found in normal proteins, but it is quite smaller than the 14% value seen in mPrP (PDB code 1ag2). This analysis rationalizes the lack of observation of scrapie formation in Dpl.

Molecular Dynamics simulations:

Helix 1 in mPrP is stable: In order to dissect the stability of PrP^C fragments that were identified using bioinformatic analysis, we used MD simulations of H1 and H2 and H3 from the PrP^C state. With the exception of residues 150-152, the propensities of the interior residues for α -helical or β -strand conformations show that the helical structure is overwhelmingly preferred. The distribution of distances between residues at positions (i,i+4) averaged over the 5 trajectories shows that, with the exception of residues in the second half of H1, the helical structure is preserved. Snapshots of typical conformations at various moments along one of the trajectories show that even the C-term end of H1, which becomes disordered after ~ 12 ns, returns to the helical conformation towards the end of the run. Small fluctuations in a short helix are unusual because it is known that isolated helices are at best marginally stable [57, 58].

In order to check if the predicted stability of H1 depends on the force field we generated 2 trajectories for a total of 40 ns using the Charmm27 parameter set with the package NAMD. The backbone rmsd with respect to the PDB structure stabilizes around 2.5-3.0 Å after ~ 10 ns. The rmsd for the backbone of the 144-149 fragment of the chain remains close to 0.5 Å for the duration of the run which is in very good agreement with the previous set of simulations. The difference between these two sets of simulations is only in the fraying of the C-terminus residues. These results, which are consistent with the MOIL simulations, also show that the fraction of helix content in H1 is high.

Mutations of residues in the second salt bridge (D147-R151) enhance conformational fluctu-

ations: The pattern searches suggest that the three (i,i+4) salt bridges ((Asp144,Arg148), (Asp147,Arg151), and (Arg148,Glu152)) in H1 should stabilize the isolated H1. To probe the importance of the second salt bridge (Asp147,Arg151), we simulated the double mutant H1[D147A,R151A]. Replacing D and R by A should not compromise the local helical propensity because Ala is the best helix-former among the amino acids [59]. Consequently, any loss of stability in the structure can be attributed largely to the loss of the the salt bridge. From relatively long MD simulations for H1[D147A,R151A], we find that the double mutant has increased conformational flexibility compared to the wild-type chain. Most residues, except position 145, have non-zero β -strand propensity.

The larger conformational fluctuations result in extended states with only the first turn of the helix still present. Based on these findings, we conclude that H1[D147A,R151A] populates two basins of attraction: one that is predominantly α -helical with a radius of gyration $\sim 6 \text{ \AA}$, and the other being mostly RC with a radius of gyration of $\sim 7.7 \text{ \AA}$. Time evolution of distances between (i,i+4) residues (data not shown) shows that the conformational change starts towards the C-terminus part of the sequence and proceeds in a highly cooperative manner. Our findings are in agreement with recent experiments [43] which showed that the peptide huPrP(140-158)D147A is destabilized compared to wt-huPrP(140-158). The decreased stability of the mutant could result in the efficient conversion of PrP^C(90-231) to the protease resistant form.

By classifying the structures generated in the MD simulations as helical [6], we find that the helical fraction, f_H , of the mutant is 0.55 while f_H for the WT is 0.64. The value of f_H is 0.63 using the Charmm parameters. We should *emphasize* that the absolute values of f_H might be overestimated and could depend upon the force field. However, meaningful conclusions can be drawn using the relative values. Using the f_H values we can estimate the free energy of stability using $\Delta F = -RT \ln(\frac{f_H}{1-f_H})$. For the WT $\Delta F_{WT} \sim -0.37 \text{ kcal/mol}$, whereas for H1[D147A,R151A] $\Delta F_M \sim -0.13 \text{ kcal/mol}$. If f_H using the Charmm parameter set is used, then $\Delta F_{WT} \sim -0.34 \text{ kcal/mol}$. The relative difference $\Delta \Delta F = \Delta F_{WT} - \Delta F_M \sim -0.24 \text{ kcal/mol}$ which arises from the salt bridge formation in WT. Interestingly, this estimate for free-energy gain due to salt bridge formation is in the range of the values reported in the literature [60].

Second half of H2 is susceptible to conformational fluctuations: The trajectories, obtained using

the NAMD package for a total of 185 ns, showed a drastic reduction in the amount of helical structure which is accompanied by an increase in β -strand content. The conformational transition starts in the second half of H2 and propagates towards its N-terminal, while H3 unwinds concomitantly at its two ends. The propensities of residues for α -helical or β -strand conformations show that only positions 178 and 179 (H2) and residues 205 to 212 (H3) maintain their native α -helical structure. The extent of the conformational transition is also reflected in the behavior of the backbone rmsd from the PDB structure (1ag2) which increases monotonically from 3 Å to 6 Å in about 5 ns and reaches 11 Å in the next 70 ns.

The conformational transitions are correlated with an increase in the angle between the axes of the two halves of H2 which changes from 20° to 90° (in the first 10 ns) followed by rapid oscillations between these values for the remainder of the trajectory. The transition is initiated in the second half of H2 where the distances between (i,i+4) positions increase from 5 to 14 Å in about 10 ns. At longer time scales ($t \sim 60$ ns) the distances between (i,i+4) residues in the first half of H2 also increase from 5 to 13 Å. These motions in H2 are correlated with fluctuations in H3, where the distances between the first four (i,i+4) pairs of residues in H3 and between positions 212 - 218 (with the exception of Cys214) increase from 5 to 13 Å in about 10 ns. Almost complete loss of helical structure occurs towards the end of the trajectory (Fig.(6)). Thus, the conclusions based on bioinformatic analysis are consistent with the results of MD simulations.

Proposed structures for PrP^{C}:* Our simulations [44] and recent experiments [42, 43] strongly suggest that H1 is unlikely to change conformation in the PrP^C \rightarrow PrP^{C*} transition. The most drastic change occurs in the second half of H2 and parts of H3. Based on the assumption that alterations in the conformation of H2+H3 do not significantly affect the rest of the protein, we have constructed a plausible ensemble of structures for PrP^{C*} (Fig.(6(b)) and 6(c)). In PrP^{C*}(90-231) obtained from the NAMD trajectories (Fig.(6(b))) the helical content is $\sim 20\%$ (a lower bound), and in PrP^{C*}(90-231) reached during the MOIL simulations (Fig.6(c)) the helical content is $\sim 30\%$ compared to 48% in mPrP^C(90-231).

The overall characteristics of these structures are consistent with those proposed by James and coworkers [37]. It remains to be seen if formation of PrP^{C*}, with fluctuating regions in

H2+H3, is required for oligomerization of PrP^C i.e., if PrP^{C*} is an on-pathway monomeric intermediate on the route to fibrillization. We should emphasize that the conformation of the prion protein in PrP^{Sc} need not coincide with PrP^{C*}.

Comparison of PrP^{C} structure with the Human prion protein dimer:* In an important paper Knaus et al. [61] announced a 2 Å crystal structure of the dimeric form of the human prion protein (residues 90-231). The structure (Fig.(7)) suggest that dimerization occurs by domain swap mechanisms in which H3 from one monomer packs against H2 from another. In fact, Eisenberg and coworkers have suggested that domain swapping mechanism may be a general route of amyloid fibril formation [62]. The electron density map seems to suggest structural fluctuations in the residues 189-198 which coincides with the maximally frustrated region predicted theoretically. The dimer interface is stabilized by residues that are in H2 in the monomeric NMR structures. The header of the PDB file of the monomeric structure of human PrP^C indicates that H2 ends at residue 194 and H3 begins at 200. The domain swapped dimer structure shows that residues 190-198 exist largely in a β -strand conformation. The $\alpha \rightarrow \beta$ transition minimizes frustration. An implication of the dimer structure is that oligomerization occurs by domain swapping which in PrP^C also might implicate the disulfide bond between Cys residues at 179 and 214. The role of the S-S bond in the PrP^{Sc} formation remains controversial. In our full-atom MD simulations of reduced mouse PrP^C (data not published), we found structures that closely resemble the monomeric structure in this dimer. For example, H1 remains mostly intact, while H2 breaks into two smaller helices, one running from its normal N-term end to position 187 and the other being formed by the C-term end residues of the original H2 and residues from the loop connecting it to H3. These findings suggest that the dimer structure is a likely route to unfolding and self-assembly of monomeric PrP^C.

Sequence pattern matches and long multiple molecular dynamics simulations of helix 1 in mPrP^C using two force fields show that the stability of H1 is due to the formation of stabilizing internal salt bridges. In view of the high propensity of α -helix observed in the isolated H1 in conjunction with supporting experimental results [41, 42, 43] it is clear that alterations in the conformation of H1 are unlikely in the PrP^C \rightarrow PrP^{C*} transition.

The predicted tendency for the second half of H2 to be involved in the formation of

PrP^{C*} is also consistent with the observation that a number of mutations at 187 and 188 (H187R, T188R, T188K, and T188A) are associated with various prion diseases. Based on our findings we proposed that regions 186-190 and 214-226 must play a central role *in the initial stages* that involve the PrP^C → PrP^{C*} transition. The large conformational change is likely to be accompanied by stretching and rotation of the two halves of H2 and by the unwinding of the N-terminal end of H3. The formation of the domain swapped structure in the dimer structure of human PrP^C [61] might be facilitated by these large scale motions.

Conclusions

The development of methods to envision the structure of amyloid fibrils has enabled us to obtain molecular insights into the assembly process itself. Computational and experimental studies are beginning to provide detailed information, at the residue level, about the regions in a given protein that harbor amyloidogenic tendencies. We have harnessed these developments to propose tentative ideas on the molecular basis of protein aggregation. These principles (or, more precisely, rules of thumb) may be useful in the interpretation and design of new experiments.

Examination of the stable structures of oligomers and fibrils obtained using experimental restraints and simulations show that these must be stable conformations which maximize the inter-peptide interactions and minimize electrostatic repulsions. Broadly, this is the only amyloid self-organization principle (ASOP) that seems to be obeyed. From the ASOP it follows that the formation of amyloid fibrils should indeed be a generic property of almost all proteins and peptides under suitable conditions. If this were the case then it is remarkable that in the case of normal function aggregation is avoided most of the time. The lack of preponderant protein aggregation may well be due to the efficiency of cleaning mechanisms operating in the cell. This may explain the lack of aggregation of PrP^{C*} under most circumstances. We conjecture that because of efficient degradation processes only mild sequence constraints are needed to prevent oligomer formation during the typical life cycle of newly synthesized proteins.

From a biophysical perspective there are a number of open problems. Are there common pathways involved in the self-assembly of fibrils? Because of the paucity of the structural description of the intermediates involved in an aggregation process a definitive answer cannot be currently provided. The energy landscape perspective, summarized briefly in Fig.(1), suggests

that multiple scenarios for assembly must exist. Although the generic nucleation and growth governs fibril formation the details can vary considerably. The microscopic basis for the formation of distinct strains in mammalian prions and in yeast prions remains a mystery. Are these merely associated with the heterogeneous seeds or are there unidentified mechanisms that lead to their growth? What factors may determine the variations in the fibrillization kinetics for the wild type and the mutants? A tentative proposal is that the kinetics of polymerization is determined by the rate of production of \mathbf{N}^* (Fig. (1)) [63], which in turn is controlled by barriers separating \mathbf{N} and \mathbf{N}^* [11, 64]. In this scenario the stability of \mathbf{N} plays a secondary role. The generality of this observation has not yet been established. Finally, how can one design better therapeutic agents based on enhanced knowledge of the assembly mechanism? Even in the case of sickle cell disease viable therapies began to emerge only long after the biophysical aspects of gelation were understood [65].

-
- [1] Selkoe, D. J. (2001) *Physiol. Rev.* **81**, 741–766.
- [2] Prusiner, S. B. (1998) *Proc. Natl. Acad. Sci. USA* **95**, 13363–13383.
- [3] Chiti, F & Dobson, C. M. (2006) *Ann. Rev. Biochem.* **75**, 333–366.
- [4] Koo, E. H, Lansbury, P. T, & Kelly, J. W. (1999) *Proc. Natl. Acad. Sci. USA* **96**, 9989–9998.
- [5] Kaye, R, Head, E, Thompson, J. L, McIntire, T. M, Milton, S. C, Cotman, C. W, & Glabe, C. G. (2003) *Science* **330**, 486–489.
- [6] Klimov, D. K & Thirumalai, D. (2003) *Structure* **11**, 295–307.
- [7] Gsponer, J, Habberth, U, & Caffisch, A. (2003) *Proc. Natl. Acad. Sci. USA* **100**, 5154–5159.
- [8] Tarus, B, Straub, J. E, & Thirumalai, D. (2005) *J. Mol. Biol.* **345**, 1141–1156.
- [9] Buchete, N. V, Tycko, R, & Hummer, G. (2005) *J. Mol. Biol.* **353**, 804–821.
- [10] Dima, R. I & Thirumalai, D. (2002) *Prot. Sci.* **11**, 1036–1049.
- [11] Dima, R. I & Thirumalai, D. (2002) *Biophys. J.* **83**, 1268–1280.
- [12] Dima, R. I & Thirumalai, D. (2004) *Bioinformatics* **20**, 2345–2354.
- [13] Harper, J. D & Lansbury, P. T. (1997) *Annu. Rev. Biochem.* **66**, 385–407.
- [14] Thirumalai, D, Klimov, D. K, & Dima, R. I. (2003) *Curr. Op. Struct. Biol.* **13**, 146–159.
- [15] Fink, A. L. (1998) *Fold. Des.* **3**, R9–R23.
- [16] Kelly, J. W. (1998) *Curr. Op. Struct. Biol.* **8**, 101–106.
- [17] Baskakov, I. V, Legname, G, Prusiner, S. B, & Cohen, F. E. (2001) *J. Biol. Chem.* **276**, 19687–19690.
- [18] Kirkitadze, M. D, Condron, M. M, & Teplow, D. B. (2001) *J. Mol. Biol.* **312**, 1103–1119.
- [19] Chien, P & Weissman, J. S. (2001) *Nature* **410**, 223–227.
- [20] Serio, T. R, Cashikar, A. G, Kowal, A. S, Sawicki, G. J, Moslehi, J. J, Serpell, L, Arnsdorf, M. F, & Lindquist, S. L. (2000) *Science* **289**, 1317–1321.
- [21] F, F. C, Webster, P, Taddei, N, Clark, A, Stefani, M, Ramponi, G, & Dobson, C. M. (1999) *Proc. Natl. Acad. Sci. USA* **96**, 3590–3594.
- [22] Ivanova, I. M, Sawaya, M. R, Gingery, M, Attinger, A, & Eisenberg, D. (2004) *Proc. Natl. Acad. Sci. USA* **101**, 10584–10589.
- [23] Klimov, D. K, Straub, J. E, & Thirumalai, D. (2004) *Proc. Natl. Acad. Sci. USA* **101**, 14760–

14765.

- [24] Miravalle, L, Tokuda, T, Chiarle, R, Giaccone, G, Bugiani, O, Tagliavini, F, Frangione, B, & Ghiso, J. (2000) *J. Biol. Chem.* **275**, 27110–27116.
- [25] Esler, W. P, Felix, A. M, Stimson, E. R, Lachenmann, M. J, Ghilardi, J. R, Lu, Y. A, V., H. V, Mantyh, P. W, Lee, J. P, & Maggio, J. E. (2000) *J. Struct. Biol.* **130**, 174–183.
- [26] Massi, F & Straub, J. E. (2001) *Biophys. J.* **81**, 697–709.
- [27] Massi, F, Klimov, D. K, Thirumalai, D, & Straub, J. E. (2002) *Protein Sci.* **11**, 1639–1647.
- [28] Zhang, S, Casey, N, & Lee, J. P. (1998) *Fold. Des.* **3**, 414–422.
- [29] Massi, F, Peng, J. W, Lee, J. P, & Straub, J. E. (2001) *Biophys. J.* **80**, 31–44.
- [30] Riek, R, Hornemann, S, Wider, G, Billeter, M, Glockshuber, R, & Wuthrich, K. (1996) *Nature (London)* **382**, 180–182.
- [31] Telling, G. C, Scott, M, Mastrianni, J, Gabizon, R, Torchia, M, Cohen, F. E, DeArmond, S. J, & Prusiner, S. B. (1995) *Cell* **83**, 79–90.
- [32] Donne, D. G, Viles, J. H, Groth, D, Mehlhorn, I, James, T. L, Cohen, F. E, Prusiner, S. B, Wright, P. E, & Dyson, H. J. (1997) *Proc. Natl. Acad. Sci. USA* **94**, 13452–13457.
- [33] Zahn, R, Liu, A, Luhrs, T, Riek, R, von Schroetter, C, Garcia, F. L, Billeter, M, Calzolari, L, Wilder, G, & Wuthrich, K. (2000) *Proc. Natl. Acad. Sci. USA* **97**, 145–150.
- [34] Haire, L. F, Whyte, S. M, Vasisht, N, Gill, A. C, Verma, C, Dodson, E. J, Dodson, G. G, & Bayley, P. M. (2004) *J. Mol. Biol.* **336**, 1175–1183.
- [35] Caughey, B. W, Dong, A, Bhat, K. S, Ernst, D, Hayes, S. F, & Caughey, W. S. (1991) *Biochemistry* **30**, 7672–7680.
- [36] Gasset, M, Baldwin, M. A, Fletterick, R. J, & Prusiner, S. B. (1993) *Proc. Natl. Acad. Sci. USA* **90**, 1–5.
- [37] Kuwata, K, Li, H, Yamada, H, Legname, G, Prusiner, S. B, Akasaka, K, & James, T. L. (2002) *Biochem.* **41**, 12277–12283.
- [38] Baskakov, I. V, Legname, G, Baldwin, M. A, Prusiner, S. B, & Cohen, F. E. (2002) *J. Biol. Chem.* **277**, 21140–21148.
- [39] Hosszu, L. P, Baxter, N. J, Jackson, G. S, Power, A, Clarke, A. R, Waltho, J. P, Craven, C. J, & Collinge, J. (1999) *Nature: Struct. Biol.* **6**, 740–743.
- [40] Kuwata, K, O.Kamatari, K, Akasaka, K, & James, T. L. (2004) *Biochem.* **43**, 4439–4446.

- [41] Liu, A, Riek, R, Zahn, R, Hornemann, S, Glockshuber, R, & Wuthrich, K. (1999) *Biopolymers* **51**, 145–152.
- [42] Speare, J. O, III, T. S. R, Bloom, M. E, & Caughey, B. (2003) *J. Biol. Chem.* **278**, 12522–12529.
- [43] Ziegler, J, Sticht, H, Marx, U. C, Muller, W, Rosch, P, & Schwarzinger, S. (2003) *J. Biol. Chem.* **278**, 50175–50181.
- [44] Dima, R. I & Thirumalai, D. (2004) *Proc. Natl. Acad. Sci. U.S.A.* **101**, 15335–15340.
- [45] DeMarco, M & Daggett, V. (2004) *Proc. Natl. Acad. Sci. USA* **101**, 2293–2298.
- [46] Chandonia, J. M, Walker, N. S, Conte, L. L, Koehl, P, Levitt, M, & Brenner, S. (2002) *Nucl. Acid. Res.* **30**, 260–263.
- [47] West, M. W, Wang, W, Patterson, J, Mancias, J. D, Beasley, J. R, & Hecht, M. H. (1999) *Proc. Natl. Acad. Sci. USA* **96**, 11211–11216.
- [48] Schwartz, R, Istrail, S, & King, J. (2001) *Protein Sci.* **10**, 1023–1031.
- [49] Kallberg, Y, Gustafsson, M, Persson, B, Thyberg, J, & Johansson, J. (2001) *J. Biol. Chem.* **276**, 12945–12950.
- [50] Rost, B & Sander, C. (1993) *J. Mol. Biol.* **232**, 584–599.
- [51] Bairoch, A & Apweiler, R. (2000) *Nucl. Acid. Res.* **28**, 275–284.
- [52] Chou, P. Y & Fasman, G. D. (1978) *Ann. Rev. Biochem.* **47**, 251–276.
- [53] Moore, R. C, Lee, I. Y, Silverman, G. L, Harrison, P. M, Strome, R, Heinrich, C, Karunaratne, A, Pasternak, S. H, Chishti, M. A, Liang, Y, Mastrangelo, P, Wang, K, A.Smit, A. F, Katamine, S, Carlson, G. A, Cohen, F. E, Prusiner, S. B, Melton, D. W, Tremblay, P, Hood, L. E, & Westaway, D. (1999) *J. Mol. Biol.* **292**, 797–817.
- [54] Nishida, N, Tremblay, P, Sugimoto, T, Shigematsu, K, Shirabe, S, Petromilli, C, Erpel, S. P, Nakaoka, R, Atarashi, R, Houtani, T, Sakaguchi, S, DeArmond, S. J, Prusiner, S. B, & Katamine, S. (1999) *Lab. Invest.* **79**, 689–697.
- [55] Mo, H, Moore, R. C, Cohen, F. E, Westaway, D, Prusiner, S. B, Wright, P. E, & Dyson, H. J. (2001) *Proc. Natl. Acad. Sci. USA* **98**, 2352–2357.
- [56] Hooft, R. W. W, Vriend, G, & Sander, C. (1996) *Nature (London)* **381**, 272–273.
- [57] Bundi, A & Wuthrich, K. (1979) *Biopolym.* **18**, 299–311.
- [58] Dyson, H & Wright, P. E. (1998) *Nat. Struct. Biol.* **5**, 499–503.
- [59] Creighton, T. E. (1993) *Proteins: Structures and molecular properties.* (W.H. Freeman and

Company, New York).

- [60] Makhatadze, G. I, Loladze, V. V, Ermolenko, D. N, Chen, X, & Thomas, S. T. (2003) *J. Mol. Biol.* **327**, 1135–1148.
- [61] Knaus, K. J, Morillas, M, Swietnicki, W, Malone, M, Surewicz, W. K, & Yee, V. C. (2001) *Nature: Struct. Biol.* **8**, 770–774.
- [62] Liu, Y, Gotte, G, Libonati, M, & Eisenberg, D. (2002) *Nature Struct. Biol.* **8**, 211–214.
- [63] Ramirez-Alvarado, M, Merkel, J. S, & Regan, L. (2000) *Proc. Natl. Acad. Sci. USA* **97**, 8979–8984.
- [64] Hammarstrom, P, Jiang, X, Hurshman, A. R, Powers, E. T, & Kelly, J. W. (2002) *Proc. Natl. Acad. Sci. USA* **99**, 16427–16432.
- [65] Eaton, W. A & Hofrichter, J. (1995) *Science* **268**, 1142–1143.
- [66] Humphrey, W, Dalke, A, & Schulten, K. (1996) *J. Mol. Graph.* **14**, 33–38.

Figure Captions

Fig.1. Schematic diagram of the two plausible scenarios of fibrillization based on free energy landscape perspective. According to scenario I, the assembly competent state \mathbf{N}^* is metastable with respect to the monomeric native state \mathbf{N} and is formed due to partial unfolding. In scenario II \mathbf{N}^* is formed upon structural conversion either of the native state \mathbf{N} (as in prions) or directly from the unfolded state \mathbf{U} (as in A β -amyloid peptides). In both cases proteins (or peptides) in \mathbf{N}^* states must coalesce into larger oligomers capable of growth into fibrils.

Fig.2. The putative dimer structures corresponding to the φ -dimer (a) and ε -dimer (b), respectively. The side chains at the dimer interface are depicted explicitly. The positively and negatively charged, polar, and hydrophobic residues are colored in blue, red, purple, and green, respectively. The C_α atoms of the monomers A (left) and B (right) are colored in cyan and yellow, respectively.

Fig.3. The Potential of Mean Force (PMF) is plotted for two different relative orientations of the monomeric peptide within the dimer. The PMF is computed as a function of the surface separation, $\delta = \xi - \xi_{cont}$, along the distance between the centers of mass (DCOMs) of the two monomers, where ξ and ξ_{cont} are the DCOMs of the two monomers when they are at an arbitrary separation and in contact, respectively. The profile in blue corresponds to the free energy surface computed using the ε -dimer as the starting structure. The red curve is similarly computed using the φ -dimer as the starting structure. The difference between the two surfaces suggests that hydrophobic interactions may be more essential to stabilization of the dimer structure than electrostatic interactions.

Fig.4. Cartoon representation of the structure of human PrP^C (PDB entry 1QLX). The three helices in the 90-231 ordered region of PrP^C are colored in red, while the short β -sheet is in yellow. The two cysteine residues (179 and 214) involved in the disulfide bond that connect H2 with H3 are indicated in bond representation and colored in purple. The C-term end of H2 and the N-term end of H3 which we believe to be implicated in the initial stages of the $\alpha \rightarrow \beta$ transition are colored in green. The figure was produced with packages VMD [66] and PovRay (<http://www.povray.org/>).

Fig.5. Cartoon representation of the structure of human Doppel protein (Dpl) (PDB entry 1LG4). The three helices in the 24-152 ordered region of Dpl are colored in red. The four cysteine

residues (94, 108, 140 and 145) involved in the two disulfide bonds that connect H2 with H3 and the loops preceding them are indicated in bond representation and colored in purple. The figure was produced with packages VMD [66] and PovRay (<http://www.povray.org/>).

Fig.6. Schematic representation of $\text{PrP}^C \rightarrow \text{PrP}^{C*}$ transition, where the conformation for PrP^C is taken from the PDB file 1ag2 (yellow). The conformations for PrP^{C*} contain H1 from 1ag2 while the residues encompassing H2+H3 are shown in a conformation (red) reached towards the end of our MD simulations using the NAMD package (6(b)) or the simulations using the MOIL package (6(c)). The schematic PrP^{C*} structures are representatives from ensembles of fluctuating conformations. In the representative PrP^{C*} structure obtained using NAMD simulations the H1 region, together with the adjacent loops and the β -strands, and residues (205-212) from H3 retain their original conformations and are therefore depicted with same color as in PrP^C . In the MOIL representative PrP^{C*} structure the H1 region, together with the adjacent loops and the β -strands, and residues (175-179), (184-188), (193,194) from H2 and residues (203-218) from H3 retain their original conformations and are therefore depicted with same color as in PrP^C . The figures are rotated such that the orientation of H1 is the same in all of them. The figures were produced with packages VMD [66] and PovRay (<http://www.povray.org/>).

Fig.7. Cartoon representation of the X-ray crystal structure of the human PrP^C dimer (PDB entry 1I4M). For each chain, A and B, the three helices in the 90-231 ordered region of PrP^C are colored in red, while the short β -sheet is in yellow. The two cysteine residues (179 and 214) involved in the disulfide bond that connect H2 with H3 are indicated in bond representation and colored in purple. The C-term end of H2 and the N-term end of H3 which we believe to be implicated in the initial stages of the $\alpha \rightarrow \beta$ transition are colored in green. We notice that, in contrast to the monomeric PrP^C structure from Fig.(4), here this region is no longer entirely helical, but contains a short stretch of β -strand structure and a shorter helix as well. The figure was produced with packages VMD [66] and PovRay (<http://www.povray.org/>).

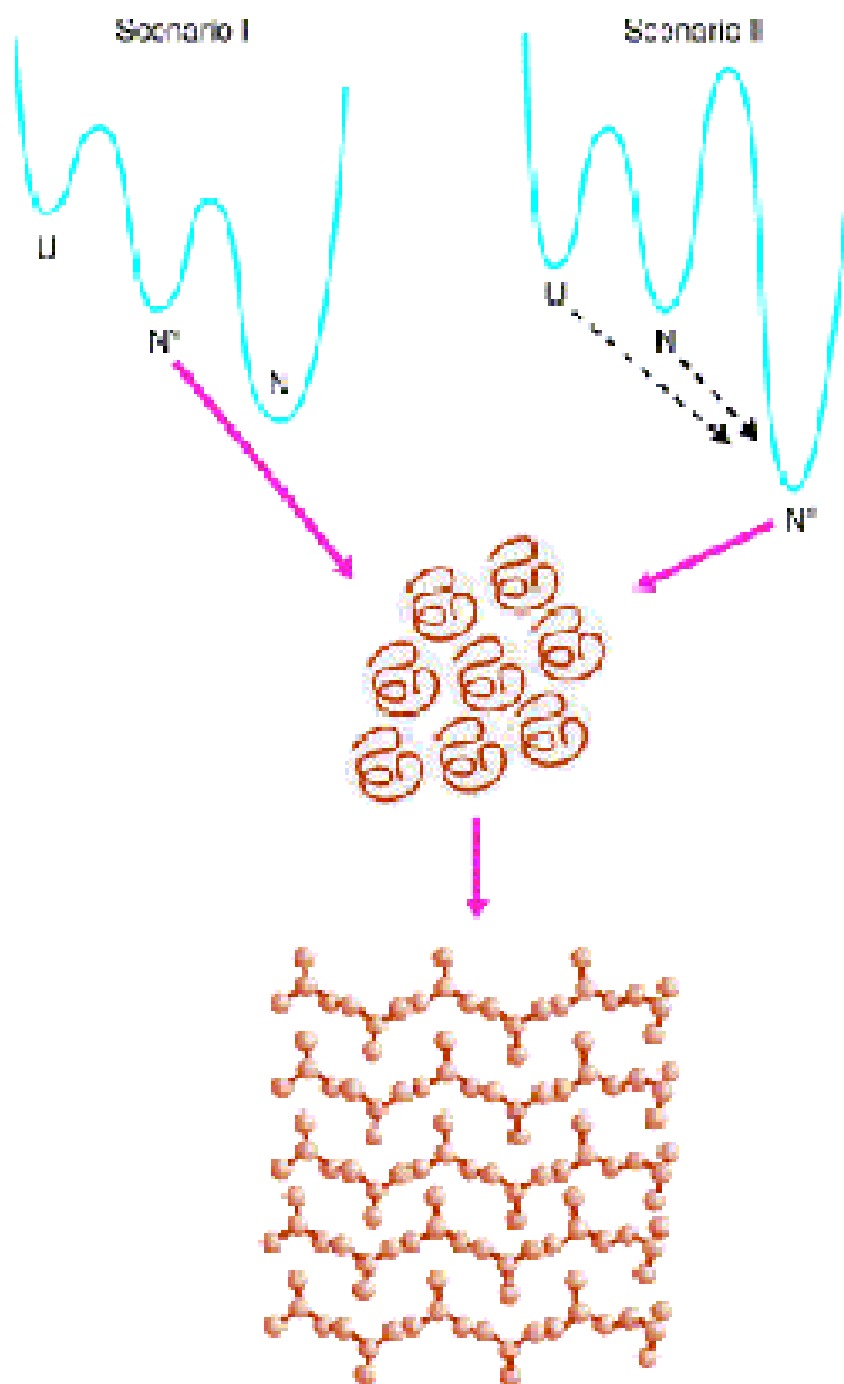
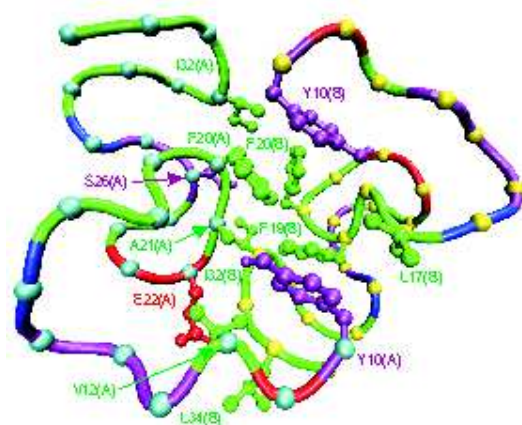


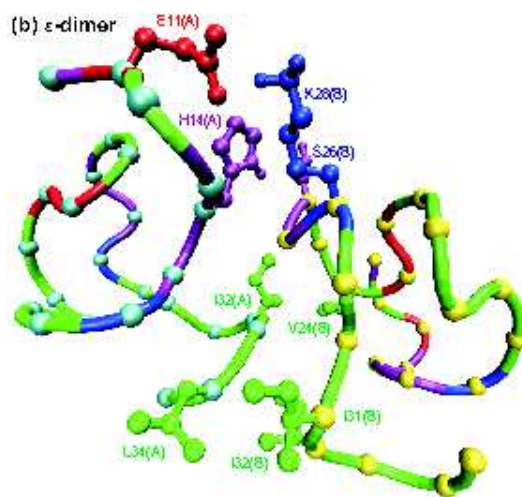
FIG. 1:

(a) ϕ -dimer



(a)

(b) ϵ -dimer



(b)

FIG. 2:

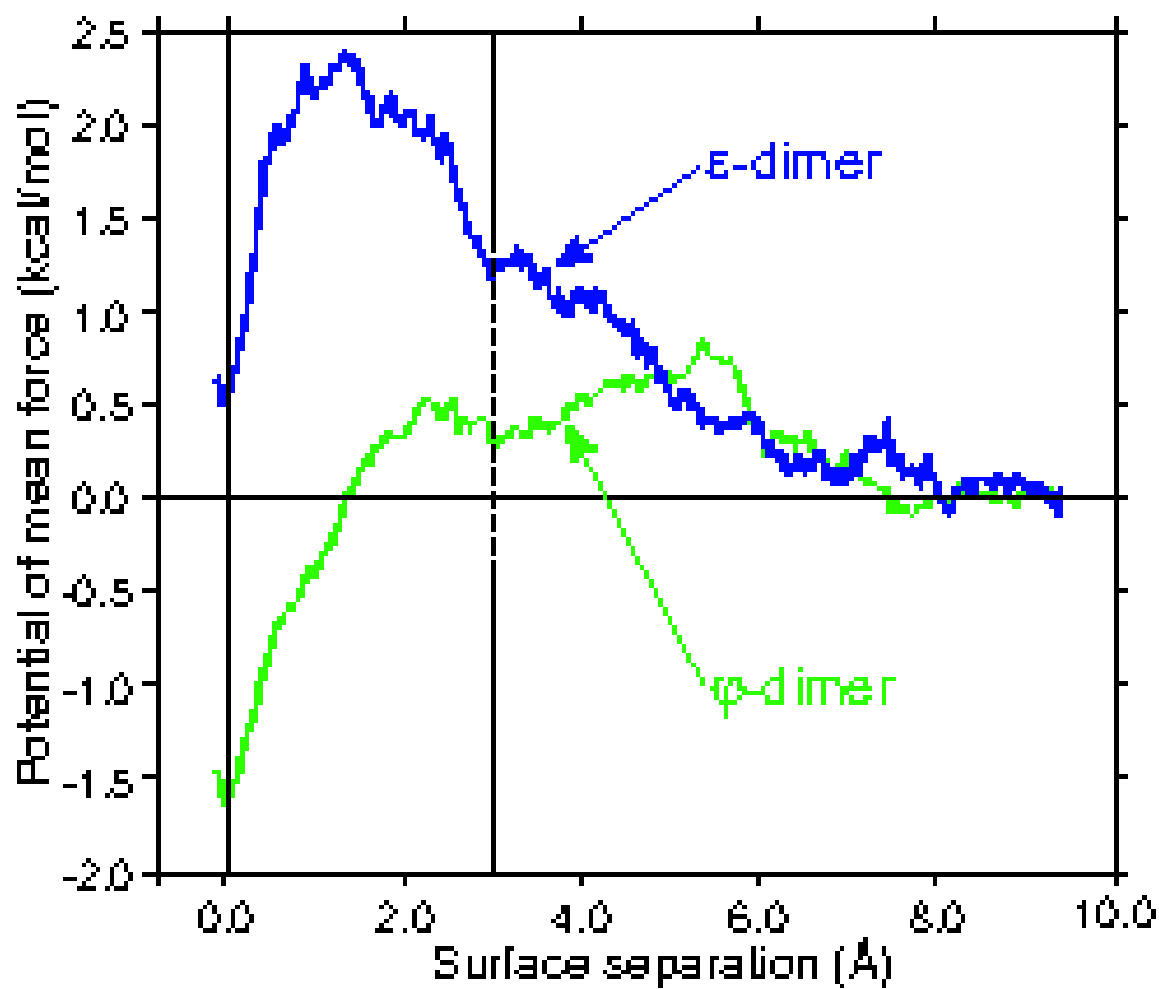


FIG. 3:

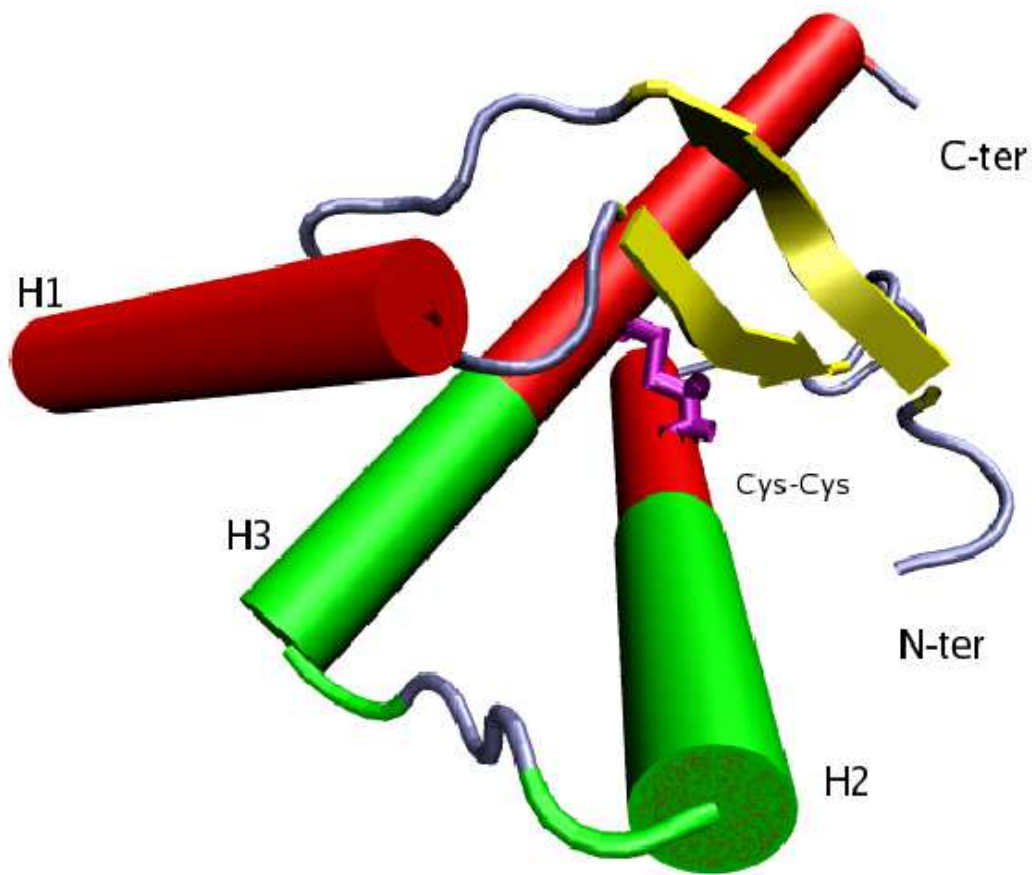


FIG. 4:

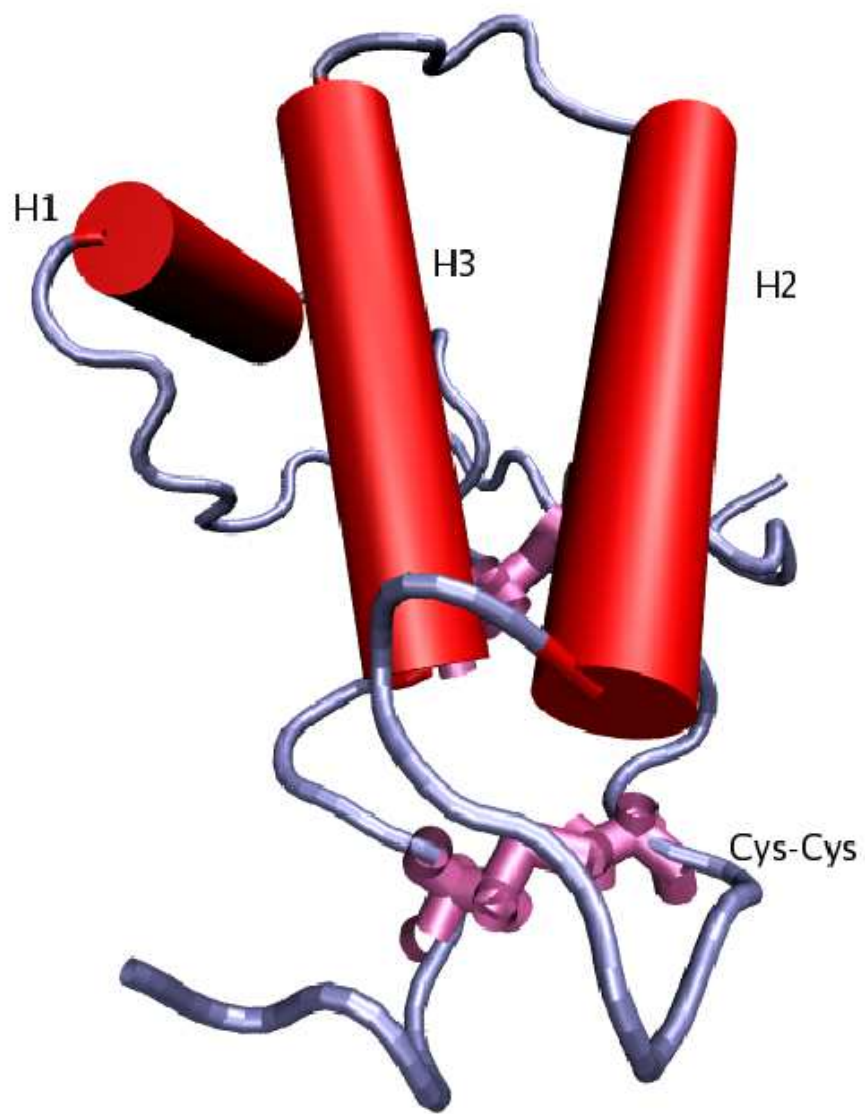
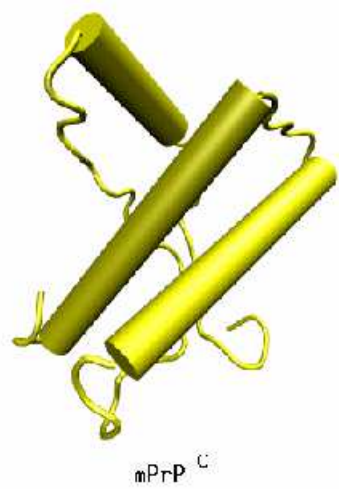
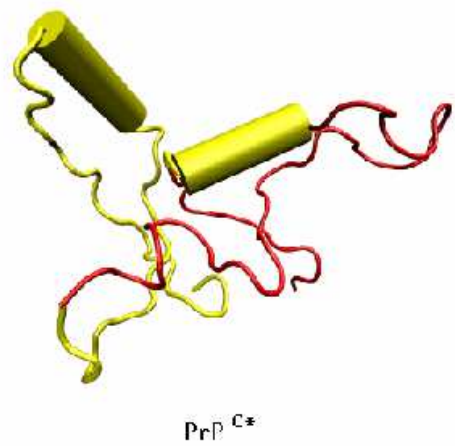


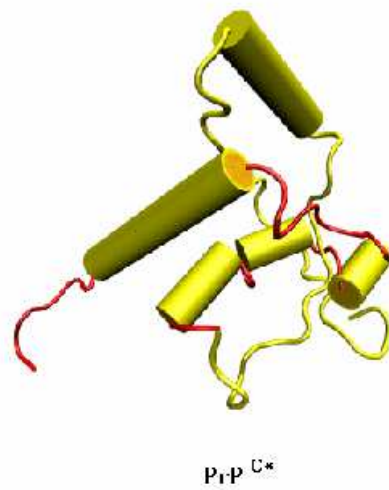
FIG. 5:



(a)



(b)



(c)

FIG. 6:

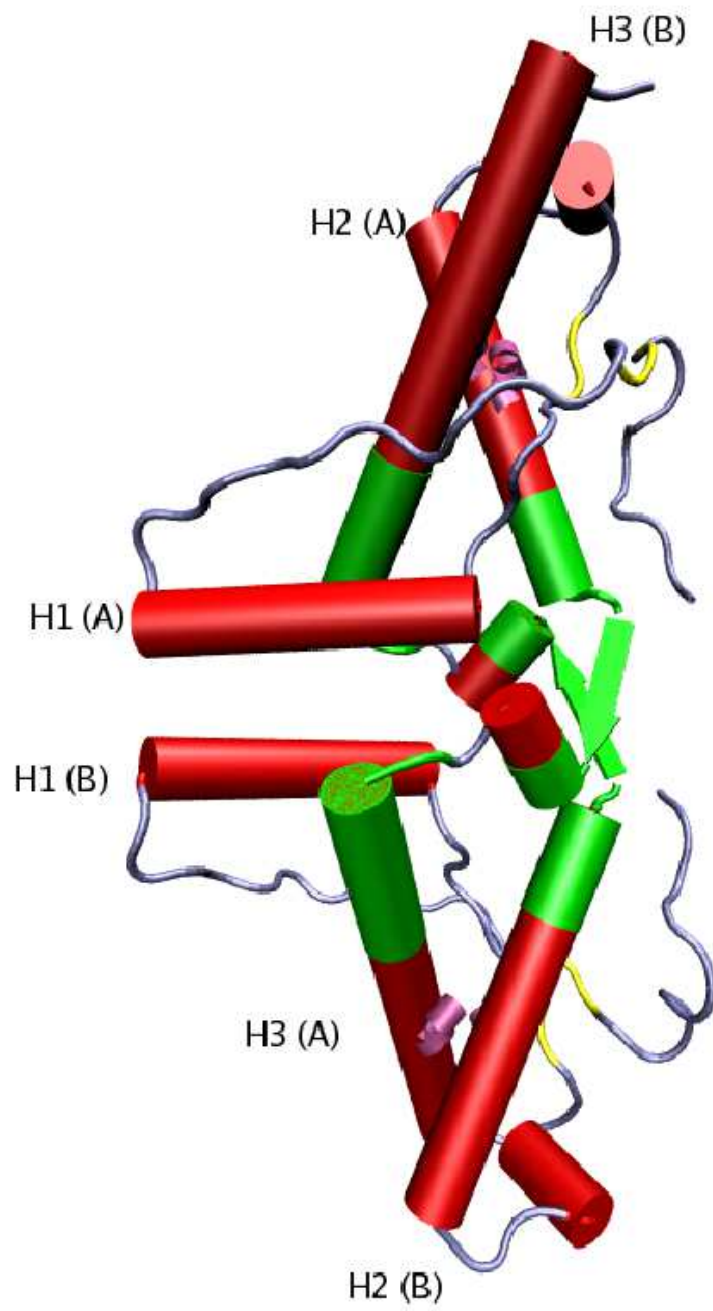


FIG. 7: